Applied Physics A (2018) 124:166
https://doi.org/10.1007/s00339-018-1584-7

Applied Physics A
Materials Science & Processing

Annealing study and thermal investigation on bismuth sulfide thin films prepared by chemical bath deposition in basic medium

O. Dachraoui[1] · J. M. Merino[2] · A. Mami[3] · M. León[2] · R. Caballero[2] · H. Maghraoui-Meherzi[1]

Received: 24 August 2017 / Accepted: 13 January 2018 / Published online: 23 January 2018
© Springer-Verlag GmbH Germany, part of Springer Nature 2018

Abstract

Bismuth sulfide thin films were prepared by chemical bath deposition using thiourea as sulfide ion source in basic medium. First, the effects of both the deposition parameters on film growth as well as the annealing effect under argon and sulfur atmosphere on as-deposited thin films were studied. The parameters were found to be influential using the Doehlert matrix experimental design methodology. Ranges for a maximum surface mass of films (3 mg cm^{-2}) were determined. A well-crystallized major phase of bismuth sulfide with stoichiometric composition was achieved at 190 °C for 3 h. The prepared thin films were characterized using grazing incidence X-ray diffraction, scanning electron microscopy and energy-dispersive X-ray analysis. Second, the bandgap energy value was found to be 1.5 eV. Finally, the thermal properties have been studied for the first time by means of the electropyroelectric (EPE) technique. Indeed, the thermal conductivity varied in the range of 1.20–0.60 W m^{-1} K^{-1}, while the thermal diffusivity values increased in terms of the annealing effect ranging from 1.8 to 3.5 10^{-7} m^2 s^{-1}.

1 Introduction

Metal chalcogenides belonging to V–VI group have been widely studied because of their excellent properties such as photoconductivity, photosensitivity and thermoelectric effect [1–4]. Among these compounds, bismuth sulfide (Bi_2S_3) is a semiconducting material whose direct bandgap energy was reported to be in the range of 1.25–1.70 eV [5, 6]. This property makes it a promising candidate for optoelectronic devices and solar applications. In fact, it has been used in liquid junction solar cells [7, 8], photodetectors [9, 10], thermoelectric devices [11] and electrochemical hydrogen storage [12]. Recently, Bi_2S_3 binary material was prepared under various nanostructures and showed interesting applications. In fact, hollow Bi_2S_3 nanospheres (NPs) were synthesized via hydrothermal process. In addition, hierarchitecture bismuth sulfide nanostructures (HNs) were fabricated by a general ionic-assisted microwave–ultrasonic combined synthetic strategy. Both materials exhibited superior Cr (VI) photoreduction capacity in real industrial wastewater [13, 14]. Furthermore, amorphous Bi_2S_3/Bi_2WO_6 heterostructure was constructed via an in-situ growth method and presented enhanced photocatalytic activity [15]. Synthesis of different morphologies of bismuth sulfide nanostructures via hydrothermal process and nanorods by microwave irradiation were also reported [16, 17]. Besides, nanowires prepared by hydrothermal technique presented high sensitivity and good stability against ethanol gas concentration down to 10 ppm [18]. Bi_2S_3 nanospheres with sizes of 212 nm were obtained by the same process. The combination of Bi_2S_3 with gentamicin showed synergistic antibacterial effect [19]. Moreover, Bi_2S_3 nanoribbons, synthesized by the solvothermal method exhibited relatively high activity for CO_2 photoreduction [20]. On the other hand, Bi_2S_3 thin film deposited by the SILAR method has been tested as a promising electrode material. Indeed, this electrode displayed a supercapacitor behavior with a specific capacitance of the order of 289 Fg^{-1} [21].

There are several chemical and physical preparation methods for bismuth sulfide thin films including thermal evaporation [22], reactive evaporation [23], Hotwall method

✉ O. Dachraoui
olfa.dachraoui@fst.utm.tn

1 Université de Tunis El Manar, Faculté des Sciences de Tunis, LR99ES15 Laboratoire de Chimie Analytique et Electrochimie, 2092, Tunis, Tunisie

2 Universidad Autónoma de Madrid, Departamento de Física Aplicada, M12, C/Francisco Tomás y Valiente 7, E-28049 Madrid, Spain

3 UR Photothermy, Photothermal Laboratory, (IPEIN), Merazka, Nabeul, Tunisia

[24], chemical vapor deposition (CVD) [25], molecular layer epitaxy (MLE) [26], successive ionic layer adsorption and reaction (SILAR) [27], self-assembled monolayer method (SAMs) [28], spray pyrolysis (SP) [29], sol–gel [30], electrodeposition [31, 32] and chemical bath deposition (CBD) [33–35].

Compared to other methods, CBD is a cost-effective technique. It offers the possibility of depositing thin films at low temperature under atmospheric conditions and does not require sophisticated instrumentation. It is also suitable for a large area of any configuration. The chemical deposition of Bi_2S_3 thin films can be carried out using different sulfide ion-releasing sources such as inorganic sources like thiosulfate or organic sources like thiourea (TU) and thioacetamide (TAM). A particular choice of sulfide precursor can lead to different structural, optical and electrical properties [36]. Moreover, few investigations using thiourea as sulfide source to prepare this thin binary sulfide have been made [8, 37, 38].

In this work, we investigated the preparation of bismuth sulfide thin films by chemical bath deposition method using thiourea as sulfide ion source varying simultaneously the principal deposition parameters such as bath temperature, deposition time and precursor concentration ratio. Doehlert matrix experimental design methodology was used to analyze their effect and possible interactions on the growth of as-prepared thin films. The annealing treatment study was carried out in argon + S_2 atmosphere. Moreover, the compositional, structural, and morphological properties of the grown thin films were studied. On the other hand, the electropyroelectric technique has been used to analyze both the thermal conductivity and diffusivity.

2 Materials and methods

2.1 Preparation of thin films

For the deposition of Bi_2S_3 thin films, bismuth nitrate ($Bi(NO_3)_3,5H_2O$) and thiourea (NH_2CSNH_2) were used, respectively, as Bi^{3+} and S^{2-} ion source precursors. Triethalonamine ($N(CH_2CH_2OH)_3$) was used as a complexing agent for the slow release of Bi^{3+} ions in the solution. Bismuth nitrate was triturated ultrasonically with triethalonamine and continuously stirred until its dissolution. Distilled water was then added under stirring to obtain a 0.1 mol L^{-1} of clear solution. The thin films were prepared by varying the volume of a 1 mol L^{-1} thiourea solution and keeping the volume of bismuth precursor solution constant. The mixture was poured in a 50 mL round-bottomed flask placed in a water bath and stirred continuously. The pH of the solution was 9. The time deposition and the temperature were varied in the preparation process. Glass microslides were used as substrates and dipped vertically in the reaction bath. They were cleaned beforehand by immersion in an aqua regia solution during 2 min and then thoroughly washed with distilled water. After the deposition, black dark films were obtained. They were ultimately washed with distilled water and dried in air.

2.2 Characterization

Structural studies were carried out using grazing incidence X-ray diffraction (GIXRD) in the range of angle 2θ between 10 and 70°. Data were collected with a PANalytical X'Pert Pro diffractometer using Cu Kα ($\lambda = 1.5418$ Å) radiation equipped with a flat graphite monochromator and a xenon detector. Detector scans with incident angles of 0.25°, 2° and 4° were performed.

Surface morphology and microstructure were studied using scanning electron microscopy (SEM) performed by a Hitachi, S-3000N that also enabled metallization by sputter Quorum, Q150T-S, for gold plating. Elemental analysis was performed by an energy-dispersive X-ray (EDX) analyzer (Oxford Instruments, Inca Xsight). The optical transmission data were recorded by means of an UV-Vis-NIR spectrophotometer CARY-17D VARIAN. The thickness was measured by a Taylor Hobson Talystep profilometer.

3 Results and discussions

3.1 Doehlert optimization for bismuth sulfide thin film growth

The effects of the main experimental parameters: temperature (U_1), precursors concentration ratio (U_2) and time deposition (U_3) on the film elaboration were investigated. The surface mass of the deposited material was used as an indicator of the films' growth study. Taking into account the possible interactions between the operating conditions, a multivariate method was used [39–41]. Doehlert matrix was selected for its interesting properties [42–45]. It presents a uniform distribution of experimental points in the studied field. It offers the possibility to explore the whole experimental domain through a minimum number of experiments. Moreover, it enables adding new factors to extend the domain without damaging the pre-existing uniformity.

Doehlert matrix for three variables can be associated to a quadratic polynomial model as indicated by the following equation:

$$Y = b_0 + \sum_{i=1}^{3} (b_i X_i + b_{ii} X_i^2) + \sum_{i<j}^{3} b_{ij} X_i X_j, \quad (1)$$

where Y represents the experimental response; b_0 is an independent term; b_i represents the coefficients of the linear

terms; b_{ii} the coefficients of the quadratic terms and b_{ij} ($i \neq j$) is the coefficient corresponding to the interaction term between i and j factors.

The coefficients of this second degree polynomial model are calculated, in the experimental region, using the least-squares method:

$$B = (X^T X)^{-1} \cdot X^T \cdot Y, \quad (2)$$

where Y is the vector of measured response, X is the model matrix, X^T the transposed model matrix and B is the vector of estimates of the coefficients.

The factors are given in the form of coded variables (X_i) without units to compare factors of different natures. The transformation of experimental values (natural variables) (U_i) into coded corresponding variables (X_i) is made on the basis of the following expression [46, 47]:

$$X_i = \frac{U_i - U_{i,0}}{\Delta U_i} \times \alpha, \quad (3)$$

where α is the coded value limit for each factor: $\alpha_1 = 1$, $\alpha_2 = 0.866$, $\alpha_3 = 0.816$.

$U_{i,0}$ is the value taken by the factor i in the centre of the experimental field concerned and ΔU_i is the range of variation of the factor i, where $U_{i,\max}$ and $U_{i,\min}$ are the maximum and minimum values of the effective variable U_i.

$$U_{i,0} = \frac{U_{i,\max} + U_{i,\min}}{2}, \quad (4)$$

$$\Delta U_i = \frac{U_{i,\max} - U_{i,\min}}{2}. \quad (5)$$

The selection of the experimental domain for each factor was made from prior experiences and knowledge of the elaboration process. The maximum and minimum values of each factor are summarized in Table 1.

In this table, R is the ratio between thiourea solution concentration and bismuth solution concentration.

The number of experiments required (N) is given by this relation $N = k^2 + k + 1$ where k is the number of variables. In the present work, $k = 3$, and therefore, the matrix was constituted of 13 experiments. The levels of independent variables (effective variables U_i) were calculated according to the following relations:

$$U_1 = 5X_1 + 80, \quad (6)$$

$$U_2 = \frac{2}{0.866} X_2 + 12, \quad (7)$$

$$U_3 = \frac{45}{0.816} X_3 + 75. \quad (8)$$

The experimental results for the three selected variables are shown in Table 2. Surface mass (SM) is the studied experimental response. It is calculated as follows:

$$\mathrm{SM} = \frac{\Delta m}{S} (\mathrm{mg\ cm^{-2}}), \quad (9)$$

where Δm represents the mass of the deposited film. It is calculated by subtracting the mass of the substrate before and after deposition. S is the surface of the deposited film.

According to obtained results, the coefficients of the polynomial model were calculated:

$$\mathrm{SM} = 3.17 + 0.058X_1 - -0.63X_2 + 1.03\,X_3 - -0.97X_1^2 - -1.57X_2^2 - 1.43X_3^2 - 1.15X_1X_2 - 0.35X_1X_3 - 1.07\,X_2X_3. \quad (10)$$

NEMRODW software (version 2002, LPRAI, Marseille, France) was used for building the experimental matrices, calculating the coefficients of the model and drawing the contour plots.

To evaluate the standard deviation of the experimental response, the experiments at the centers of the experimental domains ($X_i = 0$), (experiment number 13), were repeated two times (Table 2). The coefficient of variation (CV) also known as the relative standard deviation (RSD) calculated for the surface mass of deposited films (SM) is 1%.

Results displayed in Fig. 1 show that the most influential parameter on the films growth was the deposition time ($b_3 = 1.03$). In addition, precursor concentration ratio presented a negative effect on the response with ($b_2 = -0.63$). However, bath temperature had less weight with ($b_1 = 0.58$). Second-order effects ($b_{11} = -0.97$, $b_{22} = -1.57$, $b_{33} = -1.43$) were negative on the investigated response which means that its maximum is located in the centers of the experimental area. The temperature interaction with deposition time ($b_{23} = -1.15$), and precursor concentration ($b_{12} = -1.07$) were most important interactions with a negative effect on the response.

The results are interpreted using the predicted contour plots (curve of constant response) and the three-dimensional representations of the same plots are given in Figs. 2, 3, 4. In fact, the analysis of the isoresponse curve when precursor concentration ratio is set to $R = 12$, shows that the maximum

Table 1 Experimental region investigated

Variables	Factors	Units	Variable region	
			Minimum value	Maximum value
X_1	U_1: temperature (T)	°C	75	85
X_2	U_2: precursor concentration ratio (R)	_	10	14
X_3	U_3: time (t)	min	30	120

Table 2 Doehlert matrix and experimental plan

Experiment number	Experiment design			Experimental plan			Results
	X_1	X_2	X_3	U_1	U_2	U_3	Y; SM (mg cm^{-2})
1	1.0000	0.0000	0.0000	85	12	75	2.8
2	− 1.0000	0.0000	0.0000	75	12	75	1.6
3	0.5000	0.8660	0.0000	83	14	75	1.1
4	− 0.5000	− 0.8660	0.0000	78	10	75	1.4
5	0.5000	− 0.8660	0.0000	83	10	75	3.3
6	− 0.5000	0.8660	0.0000	78	14	75	1.2
7	0.5000	0.2887	0.8165	83	13	112	2.1
8	− 0.5000	− 0.2887	− 0.8165	78	11	38	0.5
9	0.5000	− 0.2887	− 0.8165	83	11	38	1.3
10	0.0000	0.5774	− 0.8165	80	13	38	1.1
11	− 0.5000	0.2887	0.8165	78	13	112	2.5
12	0.0000	− 0.5774	0.8165	80	11	112	3.3
13	0.0000	0.0000	0.0000	80	12	75	3.1
14	0.0000	0.0000	0.0000	80	12	75	3.2
15	0.0000	0.0000	0.0000	80	12	75	3.2

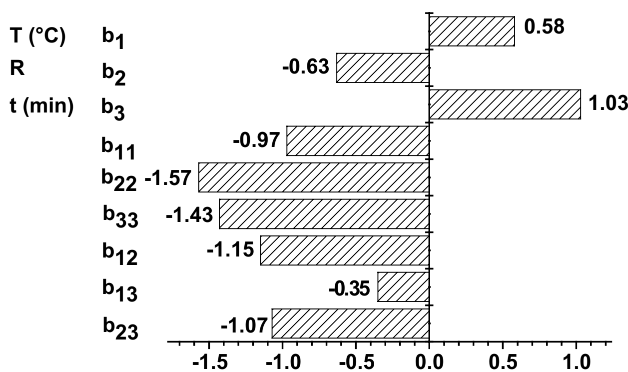

Fig. 1 Graphic analysis of effects. B_i represents the estimation of the main effects of U_i; b_{ii} the estimation of the second-order effects; b_{ij} the estimation of the interactions between U_i and U_j. [U_1: temperature (°C), U_2: precursor concentration ratio and U_3: time (min)]

of surface mass of deposited films (more than 3 mg cm^{-2}) was reached when both temperature and deposition time were increased, respectively, in the range of 78 and 84 °C in one hand, and between 66 and 114 min on the other hand (Fig. 2). Moreover, it was noted that maximum surface mass (more than 3 mg cm^{-2}) when time deposition is fixed to $t=75$ min was obtained with increasing temperature above 79 °C and precursor concentration ratio ranging from 10 to 12 (Fig. 3). Mass surface of more than 3 mg cm^{-2} is also obtained when temperature deposition value is $T=80$ °C giving a time deposition ranging from 68 to 120 min and precursors concentration ratio between 10 and 13 (Fig. 4). In conclusion, optimal surface mass for an appropriate covering of the glass substrate (more than 3 mg cm^{-2}) can be obtained when the experimental factors are chosen in these following intervals. Precursor concentration ratio selected range from 10 to 13. Deposition temperature is fixed between 78 and 84 °C. Time deposition is set between 66 and 120 min.

For a complementary test, we proceeded to the deposition of three films under specific experimental conditions to obtain a surface mass of 3 mg cm^{-2} (Table 3). Results show that the obtained surface mass values are in an acceptable confidence interval of 10%. The value differences can be explained by the possible sources of uncertainty such as the weight measurement of the sample and the deposition temperature.

3.2 Annealing study

To obtain a single phase of bismuth sulfide thin films, different annealing temperatures and times were investigated (Table 4). The samples were thermally treated in an argon + S_2 atmosphere ($P\sim700$ mbar). A heating rate of 5°C/min was used. The as-deposited samples were placed in a graphite box that was supplied by a desired amount of elemental sulfur prior to heating. A quartz tube furnace equipped with a three-zone oven that improves homogeneity in the temperature and length of the plateau at constant temperature was used. The films were elaborated at the following operating conditions: $T=84$ °C, $R=13$ and $t=90$ min. Table 4 lists the composition of as-deposited and annealed under different conditions films, measured by energy-dispersive X-ray (EDX). The results were normalized by suppressing elements like silicon (Si) and /or calcium (Ca). Grazing incidence XRD patterns of all samples were compared to standard data of bismuth sulfide (JCPDS powder diffraction card no. 00-17-0320) and bismuth oxide (JCPDS powder diffraction card no. 03-065-2366).

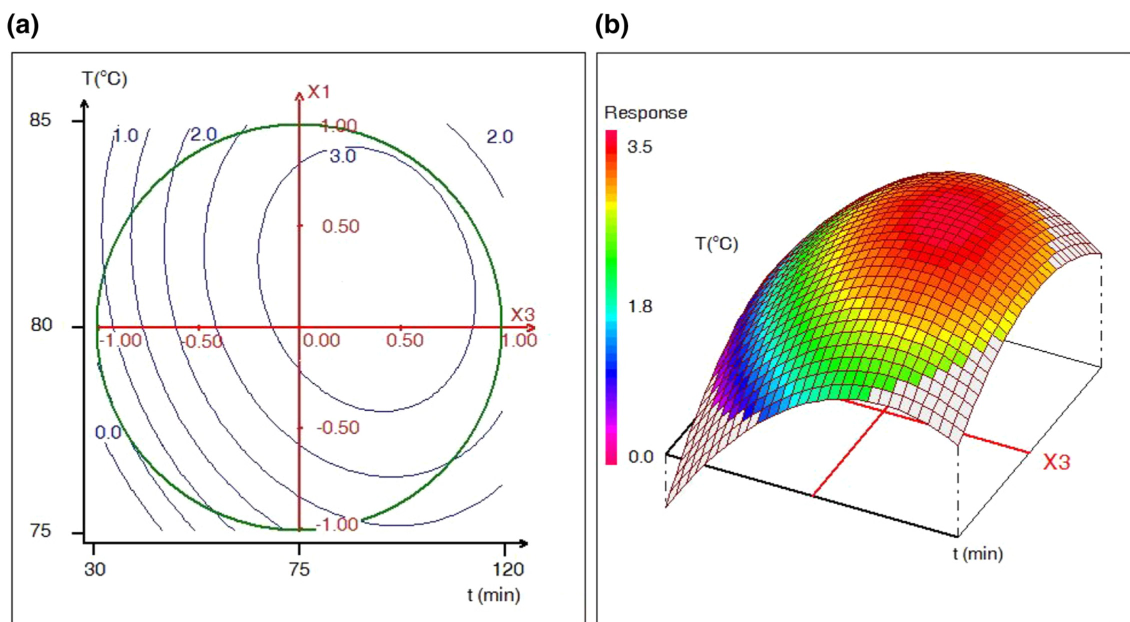

Fig. 2 **a** Contour plot of the calculated surface mass, SM (mg cm^{-2}) as a function of deposition time and temperature at fixed precursor concentration ratio $R=12$. **b** Corresponding three-dimensional representation

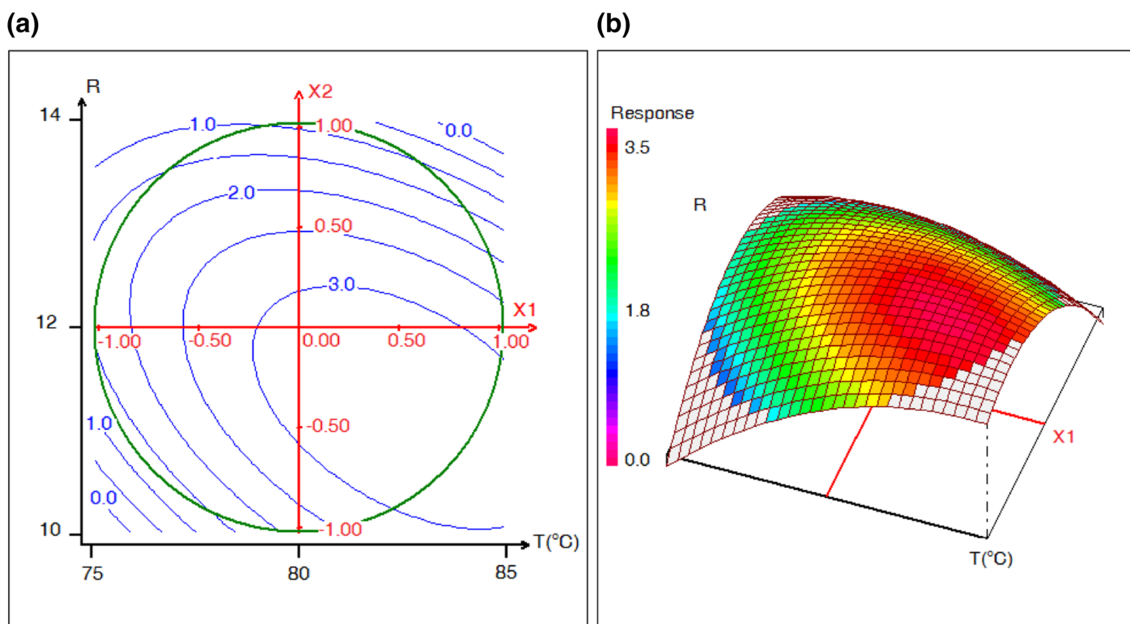

Fig. 3 **a** Contour plot of the calculated surface mass, SM (mg cm^{-2}) as a function of precursor concentration ratio and temperature at fixed time deposition $t=75$ min. **b** Corresponding three-dimensional representation

The grazing incidence XRD patterns of as-deposited sample (A) are shown in Fig. 5. The film appeared to be nearly amorphous with wide peaks. It presented a weak crystalline phase. The diffraction peaks were compared to standard data indicating the presence of a mixture of bismuth sulfide and bismuth oxide phases. It was noted that major peaks (002) and (211) are related to bismuth oxide. In fact, non-stoichiometric state was confirmed and element proportion of bismuth to sulfide was found to be 1.09 (Bi = 52.19%, S = 47.81%) (Table 4).

Annealing of sample (B) at 150 °C for 2 h showed a similar XRD pattern as the as-deposited sample. Weak crystallinity was observed (Fig. 5).However, the bismuth oxide (211) peak decreased while a characteristic peak (221) of

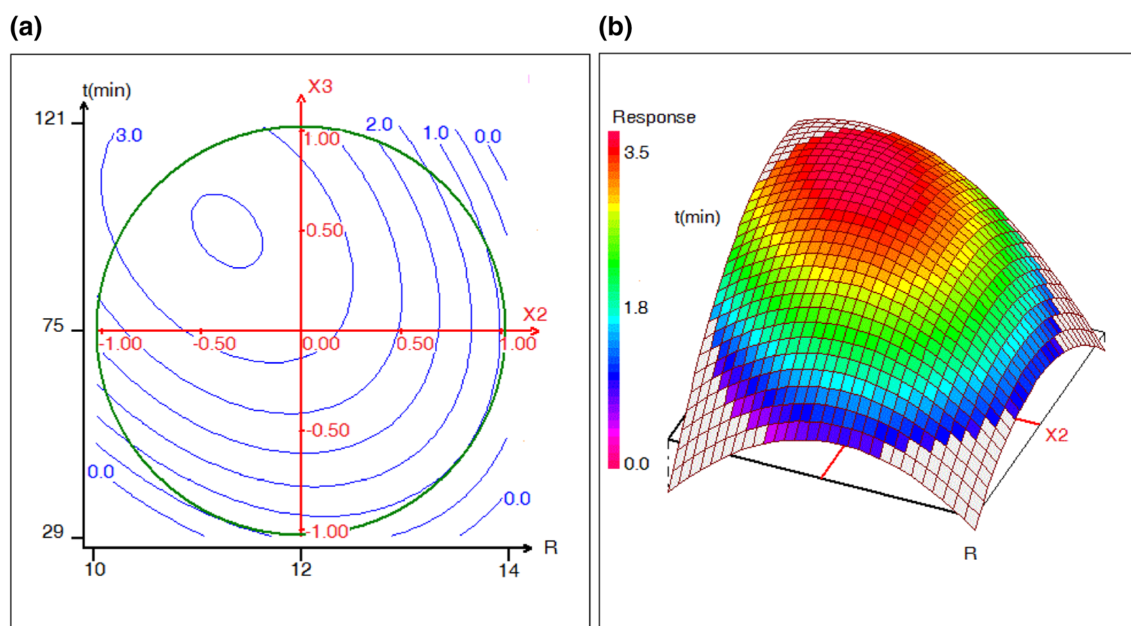

Fig. 4 **a** Contour plot of the calculated surface mass, SM (mg cm^{-2}) as a function of deposition time and precursor concentration ratio at fixed temperature $T = 80$ °C. **b** Corresponding three-dimensional representation

Table 3 Comparison experiments to obtain surface mass films of 3 mg cm^{-2}

Sample no.	1	2	3
Temperature: T (°C)	84	82	80
Precursor concentration ratio: (R)	12	12	13
Time: t (min)	75	110	90
Surface mass: SM (mg cm^{-2})	3.1	2.85	2.9

bismuth sulfide appeared. Indeed, Bi/S ratio decreased to 0.80 (Bi = 44.81%, S = 55.19%).

The annealing of samples (C) and (D), at 180 °C for 3 h with supplementary elemental sulfur of 0.1 and 0.2 g, respectively, still indicated the presence of two phases like previously mentioned (Fig. 6). However, the crystallinity increased and the number of characteristic diffraction peaks related to bismuth sulfide was noticeably increased comparing to earlier, e.g.,: (211), (220) and (101) lines. In addition, Bi/S atomic ratio decreased for both samples (C) and (D) to become 0.74. The difference in supplied amount of elemental sulfur did not have a distinct effect on composition. Longer time at $T = 180$ °C led to lower Bi/S atomic ratio from 0.74 to 0.67 for 3 to 4 h which could be an indication of a better interdiffusion of Bi-S. However, GIXRD patterns of sample (E) remained similar to those of samples (C) and (D) (Fig. 6).

It is worth noting that the transformation from nearly amorphous state to good crystallinity occurred during annealing at 190 °C for 3 h with additional 0.2 g of elemental sulfur (Fig. 7). All diffraction peaks in the pattern were labeled and indexed. It was found to be in good agreement with the orthorhombic structure of bismuth sulfide.

The pattern displayed characteristic peaks of Bi_2S_3: (220), (130), (211) and (221) at 22.39°, 24.99°, 28.61°, 31.80°, respectively, with a preferential orientation in the (130) plane. The average crystallite size of the film was

Table 4 EDX analysis of an as-deposited thin film and different annealing conditions

Sample	Temperature (°C)	Time (h)	S (g)	Bi (at%)	S (at%)	Bi/S
A	As deposited			52.19	47.81	1.09
B	150	2	0.06	44.81	55.19	0.80
C	180	3	0.10	42.56	57.44	0.74
D	180	3	0.20	42.69	57.31	0.74
E	180	4	0.20	40.03	59.97	0.67
F	190	3	0.20	39.61	60.39	0.66

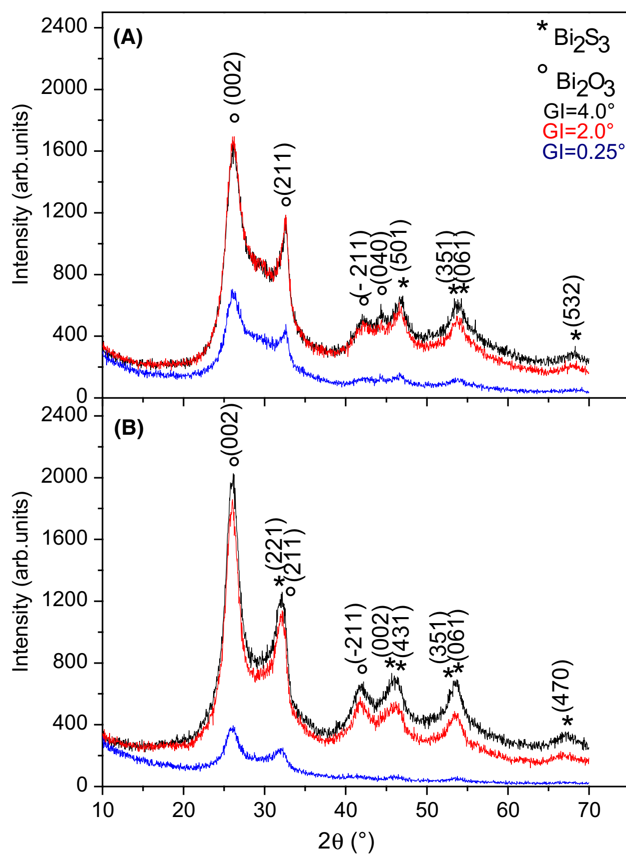

Fig. 5 GIXRD patterns of **a** as-deposited thin film and **b** annealed at 150 °C for 2 h supplied with 0.06 g of elemental sulfur

determined from lines (130), (211) and (221) using the Scherrer formula:

$$d = \frac{K\lambda}{\text{FMWH} \times \cos\theta}, \tag{11}$$

where FMWH is the full width at half maximum of the diffraction peak, λ is the wavelength of X-rays ($\lambda = 1.541874 \times 10^{-10}$ m), θ is the Bragg angle and K is the Scherrer constant and taken in this case as 0.90. The average crystallite size value was found to be around 22 nm.

A minor secondary phase was still detected. Two diffraction peaks with low intensity related to bismuth oxide remained. The chemical composition, checked by energy-dispersive X-ray analysis (EDX), shows the stoichiometry of the sample (F). The element proportion of bismuth to sulfide was found to be close to 2:3 with Bi: 39.61% and S: 60.39%, which is in good agreement with the stoichiometric ratio of bismuth sulfide.

SEM cross-sectional views of samples (A) and (E) are shown in Fig. 8. It can be seen that films contained random distribution of spherical small crystallites. A duplex structure was observed with a compact inner thin film and an outer porous layer with crystallite overgrowth. The two structures

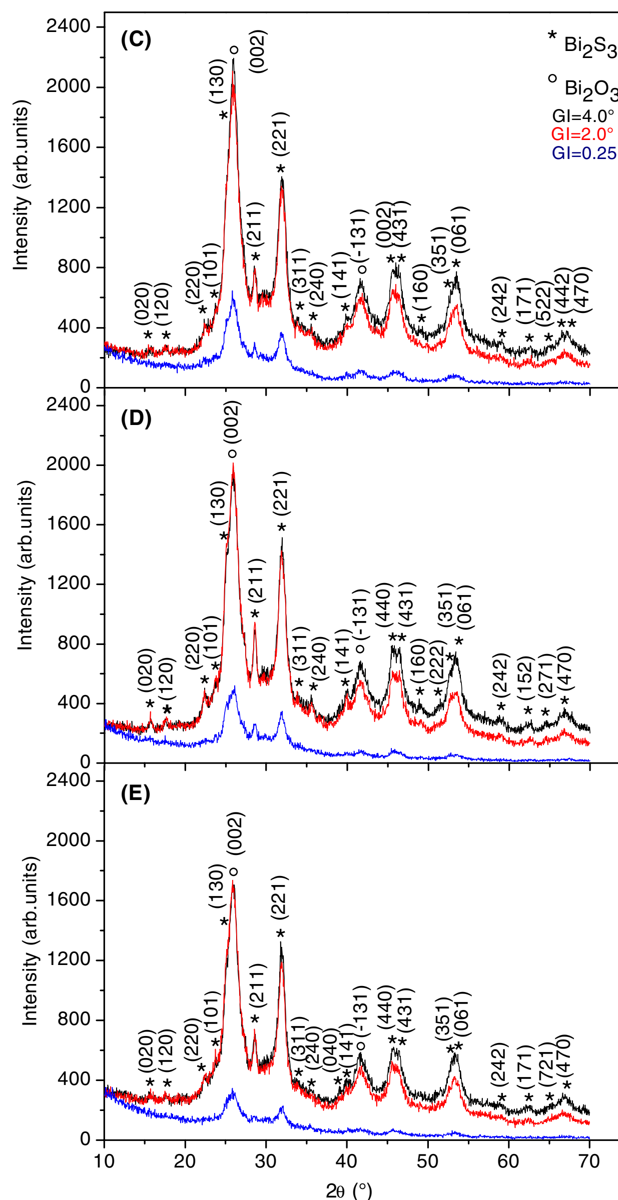

Fig. 6 GIXRD patterns of **c**–**e** thin films annealed, respectively, at 180 °C for 3 h supplied, respectively, with 0.1 and 0.2 g of elemental sulfur and at 180 °C for 4 h supplied with 0.2 g of elemental sulfur

were different in terms of composition. In fact, EDX measurements on specific localizations showed for sample (F) an inner layer composition of Bi: 41.03% and S: 58.97%. However, the outer overgrowth composition was Bi: 38.27% and S: 61.73%. An ion by ion process could be an explanation of the formation of the inner film. Whereas the presence of aggregates on the surface may be due to the parallel homogenous precipitation reaction from the colloids contained in the solution from a cluster-by-cluster mechanism similar to chemically deposited CdS thin films reported elsewhere [48]. It could be also explained by the catalytic role of the inner phase that would

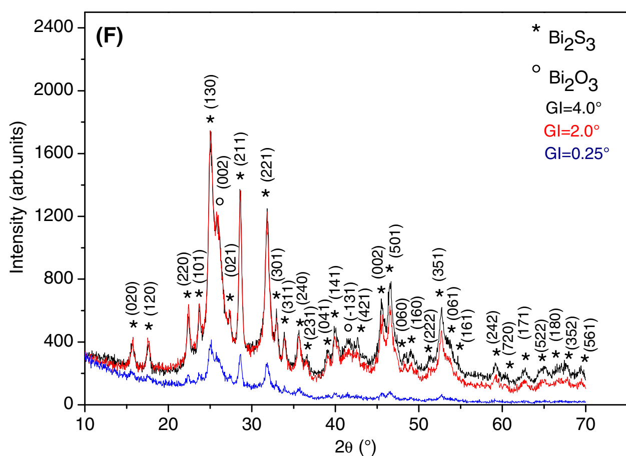

Fig. 7 GIXRD pattern of **f** thin film annealed at 190 °C for 3 h supplied with 0.2 g of elemental sulfur

where Eg is the optical bandgap and $n = 2$, 1/2, 2/3 for allowed direct, allowed indirect and forbidden direct transitions, respectively, α is the absorption coefficient at frequency ν and A is a constant. The linear nature of the plot indicates the existence of a direct transition. The bandgap is determined by extrapolating the straight portion of the plot to the energy axis (Fig. 9). This gives an energy bandgap equal to 1.5 eV which is consistent with the previous works [8, 52].

This estimated value is higher than the corresponding Eg for bulk Bi_2S_3, that is listed as 1.3 eV [53]. It can be explained by the defects, charged impurities, disorder at the grain boundaries and differences in stoichiometry, which could increase the energy bandgap with the decrease of particle size [27].

lead to further preferential deposition as previously proposed for CdSe and PbSe films [49].

The optical properties of sample (F) annealed in optimal conditions were studied by measuring the transmission spectrum in the 1500–500 nm range. No specular reflectivity spectra could be measured in these samples in this region, their values lying within the instrumental error, nor any diffuse reflectivity, because of the low reflectance of the samples and their porosity. The optical absorption coefficient (α) was then calculated using the usual expression [50, 51]:

$$\alpha = -\frac{1}{e}\ \ln(T), \tag{12}$$

where e is the film thickness.

The bandgap can be determined using the following empirical relation:

$$\alpha = \frac{A\ (h\nu - \mathrm{Eg})^n}{h\nu}, \tag{13}$$

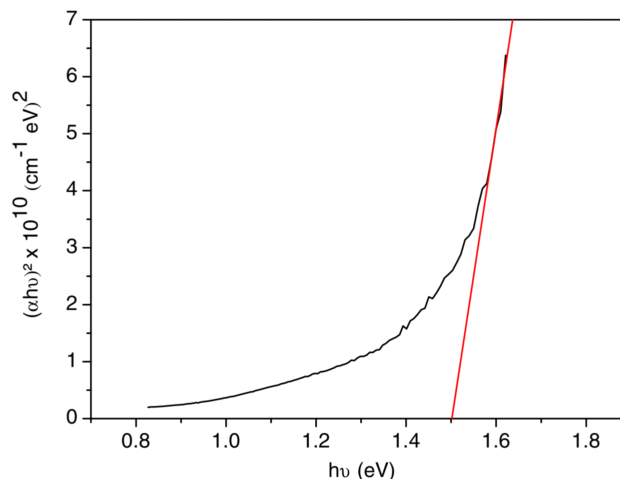

Fig. 9 Plots of $(\alpha h\nu)^2$ vs. $(h\nu)$ for Bi_2S_3 film (Sample F) with a thickness of 0.4 µm

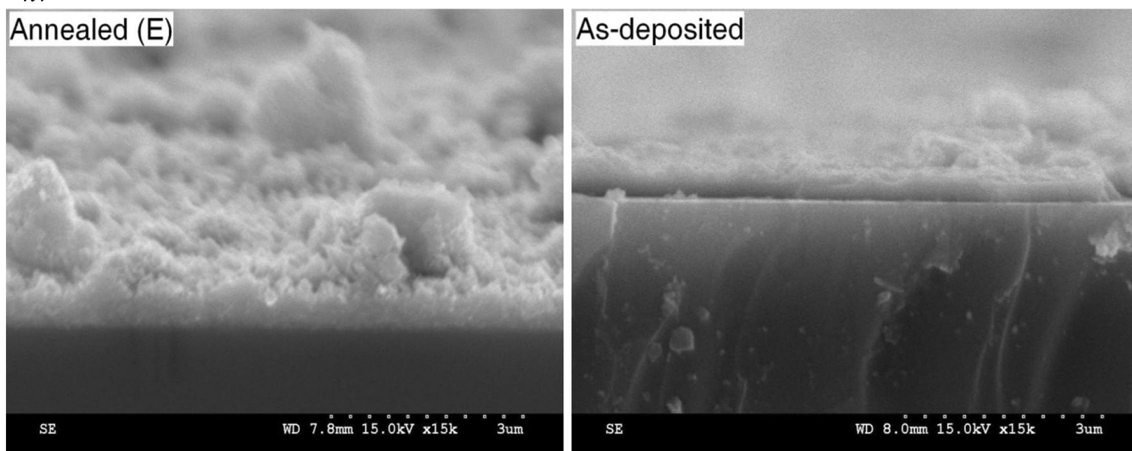

Fig. 8 Cross-sectional SEM micrographs of the as-deposited thin film (**a**), and annealed thin film (**e**) at $T = 180$ °C for 4 h supplied with 0.2 g of elemental sulfur. Operation voltage = 15 kV and magnification = 15 K × have been used, samples were gold plated

3.3 Electropyroelectric investigation

3.3.1 Experimental conditions

Given that in the field of thermoelectricity there is the tendency to employ compounds with heavy elements to keep the thermal conductivity low; this work carries important implications on the entire class of metal sulfides as candidate materials for thermoelectric applications. This is important from the point of view of environmental compatibility and materials costs. In this paper, an electropyroelectric (EPE) technique has been used to reach both the thermal conductivity and diffusivity [54].

In the EPE experiments, a voltage generator provides a sinusoidal-modulated voltage through the serpentine at metal contact. An oscillatory heat flux via the joule effect diffuses through silpad 900S which acts as an electrical insulator and a thermal conductor concurrently to insure short-circuit protection. A temperature gradient will be induced at a PVDF film, (PolyVinyliDene Fluoride) of 28-µm-thick, for which the bottom surface is thermally attached to the investigated thin film. The EPE signal data (amplitude and phase) were connected to a preamplifier, a Stanford SR 530 lock-in amplifier and a computer controlled via an RS 232 interface. The frequency range used in EPE experiment is about 10 Hz until the degradation of the signal/noise ratio is significant and Silpad 900S becomes electrically conductive. We made numerical simulations and experimental measurements using the simulation program (Maple.12). Afterwards, the simulation curves were processed and inversed by Microcal Origin 8.0. In our case, thermal parameters of air, PVDF, Silpad 900S and glass are gathered in Table 5 [55].

In this electropyroelectric method, the front detection configuration has been considered. Indeed, Fig. 10 displays this configuration that is made of five adjacent layers: air (a), an insulator sample (2), a PVDF film (p), the investigated sample (1), the substrate (S) and a backing (b).

The theoretical model of the EPE-normalized voltage signal is a complex function of the root of frequency modulation and properties of the components of the detector. Finally, thermal effusivity e and volume heat capacity C can be obtained from the following equations, where k is the thermal conductivity and D the thermal diffusivity:

Table 5 Thermal parameters of air, PVDF, Silpad 900S and glass

	Thermal effusivity e ($J\ K^{-1}\ m^{-2}\ s^{-1/2}$)	Thermal diffusivity D ($m^2\ s^{-1}$)
Air	5.81	2×10^{-5}
Silpad 900S	6105.604	7×10^{-8}
PVDF	559.4309	5.4×10^{-8}
Glass	1230.365	5×10^{-7}

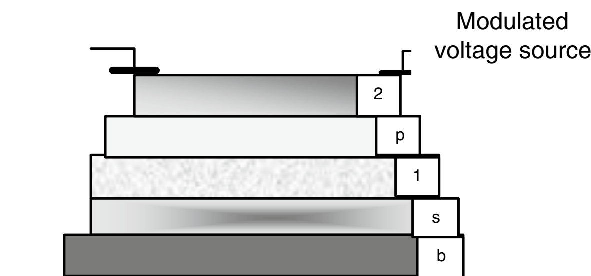

Fig. 10 Geometry of electropyroelectric cell in front detection configuration

$$e = \frac{k}{\sqrt{D}}, \tag{14}$$

$$C = \frac{k}{D}. \tag{15}$$

3.3.2 Thermal characterization

Figures 11, 12 and 13 show the best fit found between experimental and theoretical amplitudes and phases of the normalized EPE signal as a function of modulation frequency for samples (A), (E) and (F) (Table 4). The best coincidences between these curves are obtained for given values of both thermal conductivity k and thermal diffusivity D values for the studied sample. Then, we rely on Eqs. (14) and (15) to finish determining remaining thermal effusivity and heat capacity. The obtained values are listed in Table 6.

The thermal conductivity for all the samples shows the same decreasing trend with increasing measurement temperature (Table 6), which is ascribed to the strong phonon

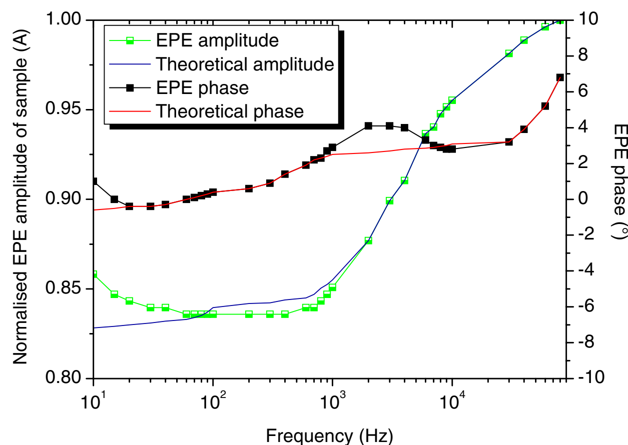

Fig. 11 Experimental (dots) and theoretical (line) normalized amplitude and phase of the electropyroelectric signal according to the frequency modulation for as-deposited sample (A)

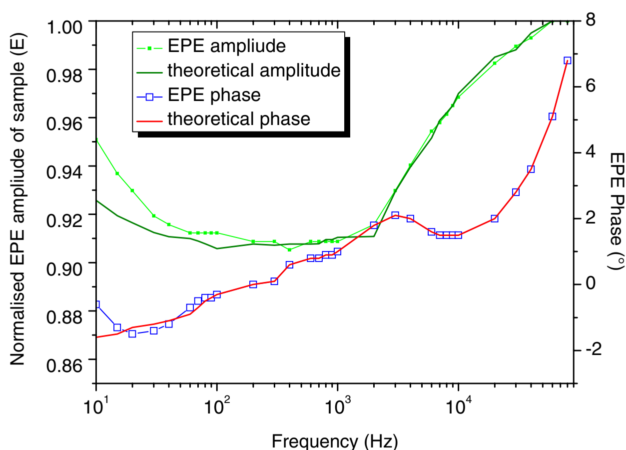

Fig. 12 Experimental (dots) and theoretical (line) normalized amplitude and phase of the electropyroelectric signal according to the frequency modulation for annealed sample (E)

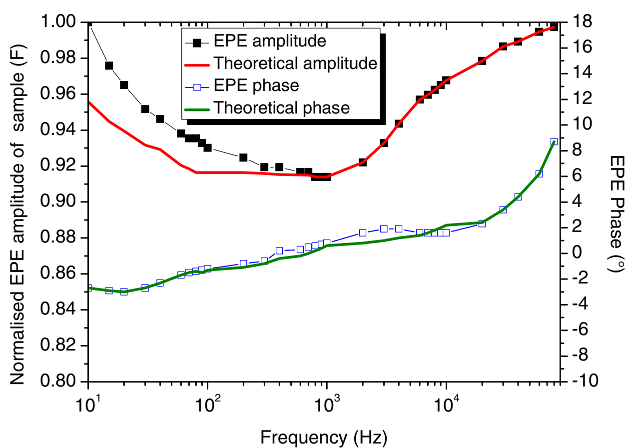

Fig. 13 Experimental (dots) and theoretical (line) normalized amplitude and phase of the electropyroelectric signal according to the frequency modulation for annealed sample (F)

scattering at high temperature. As expected, annealing significantly improves the thermoelectric properties for its low thermal conductivity (< 1.5 W m^{-1} K^{-1}), which are best for the samples prepared with the smallest particle sizes.

Compared with the thermal conductivity at room temperature for Bi_2S_3 polycrystalline materials (1.3 W m^{-1} K^{-1}) [56], we note that the thermal conductivity of as-deposited sample A is well comparable to this value. The difference between the values extracted from EPE technique and those reported in the literature can be explained by the effects of thermal resistances at the interfaces between different layers and the presence of optical large noise levels.

The surprising low thermal conductivity of the sample (F) makes it a good candidate material for thermoelectric applications. Unfortunately, thermal diffusivity, heat capacity and thermal effusivity measurements on chemically synthesized and annealed bismuth sulfide thin films have not been reported up to date. Therefore, comparison with experimental data from other sources is impractical. The thermal diffusivity of bismuth sulfide samples ranging from 1.8 to 3.5 (10^{-7} m^2 s^{-1}) are well comparable to or even lower than that of Bi_2Te_3 compounds [57].

4 Conclusion

In this study, bismuth sulfide Bi_2S_3 thin films were deposited by chemical bath deposition on glass substrate using thiourea as sulfide precursor in basic medium. Doehlert matrix allowed determining the optimal working ranges of conditions for a maximum surface mass of thin films (3 mg cm^{-2}). It can be attained using a temperature in the range of 78–84 °C, a time deposition in the range of 68–120 min and a ratio of precursor concentration within the range of 10–13. Both GIXRD measurements and EDX measurements showed that as-prepared films exhibited a nearly amorphous state and indicated the presence of a secondary phase of bismuth oxide. However, an optimum choice of the annealing condition at 190 °C during 3 h in sulfur atmosphere allows obtaining a major phase of bismuth sulfide that exhibits a well-crystallized orthorhombic structure in good agreement with stoichiometric composition. Its bandgap energy was estimated to 1.5 eV. This study seems interesting since a cost-effective process has been used to obtain bismuth sulfide thin films for a possible application in thermoelectric domain due its low thermal conductivity 0.6 ± 0.04 (W m^{-1} K^{-1}). Further studies are in progress to test these films in sensitivity applications such as photocatalysis and gas sensors.

Table 6 Thermal parameters of the samples

Sample	Thermal conductivity k (W m^{-1} K^{-1})	Thermal diffusivity D (10^{-7} m^2 s^{-1})	Heat capacity C (10^4 J K^{-1} m^{-3})	Thermal effusivity e (J K^{-1} m^{-2} $s^{-1/2}$)
Sample (A)	1.20 ± 0.04	1.80 ± 0.05	666.66	2828.43
Sample (E)	0.90 ± 0.04	2. 10 ± 0.05	428.57	1963.96
Sample (F)	0.60 ± 0.04	3.50 ± 0.05	171.43	1014.18

Acknowledgements The authors are grateful to the Interdepartmental Investigation Service (SIdI), Autonomous University of Madrid, Spain, for providing SEM, EDX and GIXRD facility. This work was financially supported by the Tunisian Ministry of Higher Education and Scientific Research and by the WINCOST (ENE2016-80788-C5-2-R) project funded by the Spanish Ministry of Economy and Competitiveness.

References

1. D. Arivuoli, F.D. Gnanam, P. Ramasamy, J. Mater. Sci. Lett. **7**, 711 (1988)
2. L. Huang, P.K. Nair, M.T.S. Nair, R.A. Zingaro, E.A. Meyers, Thin Solid Films. **268**, 49 (1995)
3. M.E. Rincón, R. Suárez, P.K. Nair, J. Phys. Chem. Solids. **57**, 1947 (1996)
4. L.-D. Zhao, B.-P. Zhang, W.-S. Liu, H.-L. Zhang, J.-F. Li, J. Solid State Chem. **181**, 3278 (2008)
5. L.M. Peter, J. Electroanal. Chem. **98**, 49 (1979)
6. E. Pineda, M.E. Nicho, P.K. Nair, H. Hu, Sol. Energy. **86**, 1017 (2012)
7. B. Miller, A. Heller, Nature. **262**, 680 (1976)
8. R.N. Bhattacharya, P. Pramanik, J. Electrochem. Soc. **129**, 332 (1982)
9. D.J. Desale, S. Shaikh, F. Siddiqui, R. Birajdar, R. Late, A. Ghule, R. Sharma, Comp. Part B Eng. **46**, 1 (2013)
10. G. Konstantatos, L. Levina, J. Tang, E.H. Sargent, Nano Lett. **8**, 4002 (2008)
11. Z. Liu, J. Liang, S. Li, S. Peng, Y. Qian, Chem. Eur. J. **10**, 634 (2004)
12. R. Jin, G. Li, Y. Xu, J. Liu, G. Chen, Int. J. Hydrogen Energy. **39**, 356 (2014)
13. S. Luo, F. Qin, H. Zhao, Y. Liu, R. Chen, J. Hazard. Mater. **340**, 253 (2017)
14. R. Wang, G. Cheng, Z. Dai, J. Ding, Y. Liu, R. Chen, Chem. Eng. J. **327**, 371 (2017)
15. Q. Zhang, Z. Dai, G. Cheng, Y. Liu, R. Chen, Ceram. Int. **43**, 11296 (2017)
16. M. Salavati-Niasari, D. Ghanbari, F. Davar, J. Alloys Compd. **488**, 442 (2009)
17. J. Wu, F. Qin, G. Cheng, H. Li, J. Zhang, Y. Xie, H.-J. Yang, Z. Lu, X. Yu, R. Chen, J. Alloys Compd. **509**, 2116 (2011)
18. X. Yang, S. Tian, R. Li, W. Wang, S. Zhou, Sens. Actuators B. **241**, 210 (2017)
19. L. Ma, J. Wu, S. Wang, H. Yang, D. Liang, Z. Lu, J. Inorg. Biochem. **168**, 38 (2017)
20. J. Jin, T. He, Appl. Surf. Sci. **394**, 364 (2017)
21. S.S. Raut, J.A. Dhobale, B.R. Sankapal, Phys. E **87**, 209 (2017)
22. M.E. Rincón, M. Sánchez, P.J. George, A. Sánchez, P.K. Nair, J. Solid State Chem. **136**, 167 (1998)
23. J. Lukose, B. Pradeep, Solid State Commun. **78**, 535 (1991)
24. P.A. Krishna Moorthy, J. Mater. Sci. Lett. **3**, 551 (1984)
25. M.E. Rincón, P.K. Nair, Semicond. Sci. Technol. **12**, 467 (1997)
26. T. Öznülüer, Ü Demir, J. Electroanal. Chem. **529**, 34 (2002)
27. A.U. Ubale, A.S. Daryapurkar, R.B. Mankar, R.R. Raut, V.S. Sangawar, C.H. Bhosale, Mater. Chem. Phys. **110**, 180 (2008)
28. S.-C. Liufu, L.-D. Chen, Q. Yao, C.-F. Wang, J. Phys. Chem. B. **110**, 24054 (2006)
29. Z. Kebbab, N. Benramdane, M. Medles, A. Bouzidi, H. Tabet-Derraz, Sol. Energy Mater. Sol. Cells. **71**, 449 (2002)
30. Y. Hui, H. Dijie, J. Zhonghong, D. Yong, J. Sol-Gel Sci. Technol. **3**, 235 (1994)
31. M. Saitou, R. Yamaguchi, W. Oshikawa, Mater. Chem. Phys. **73**, 306 (2002)
32. M. Riahi, C. Martínez-Tomás, S. Agouram, A. Boukhachem, H. Maghraoui-Meherzi, Thin Solid Films. **626**, 9 (2017)
33. C.D. Lokhande, A.U. Ubale, P.S. Patil, Thin Solid Films. **302**, 1 (1997)
34. R. Mane, J. Desai, O.-S. Joo, S.-H. Han, Int. J. Electrochem. Sci. **2**, 141 (2007)
35. A.U. Ubale, Mater. Chem. Phys. **121**, 555 (2010)
36. J.D. Desai, C.D. Lokhande, Mater. Chem. Phys. **41**, 98 (1995)
37. P. Pramanik, R. Bhattacharya, J. Electrochem. Soc. **127**, 2087 (1980)
38. S. Mahmoud, FIZIKA A. **5**, 153 (1996)
39. G.E. Box, W.G. Hunter, J.S. Hunter, *Statistics for Experimenters: an Introduction to Design, Data Analysis, and Model Building*, (JSTOR, New York, 1978)
40. G.E. Box, N.R. Draper, *Empirical Model-Building and Response Surfaces*, (Wiley, New York, 1987)
41. H. Pińkowska, E. Oliveros, Ind. Eng. Chem. Res. **53**, 1320 (2014)
42. D.H. Doehlert, Appl. Stat.. **19**, 231 (1970)
43. A. Ouejhani, F. Hellal, M. Dachraoui, G. Lallevé, J.F. Fauvarque, J. Hazard. Mater. **157**, 423 (2008)
44. A.K. Abdessalem, N. Oturan, N. Bellakhal, M. Dachraoui, M.A. Oturan, Appl. Catal., B. **78**, 334 (2008)
45. A. Hannachi, S. Hammami, N. Raouafi, H. Maghraoui-Meherzi, J. Alloys Compd. **663**, 507 (2016)
46. S.L.C. Ferreira, W.N.L. dos Santos, C.M. Quintella, B.B. Neto, J.M. Bosque-Sendra, Talanta. **63**, 1061 (2004)
47. S. Hammami, A. Ouejhani, N. Bellakhal, M. Dachraoui, J. Hazard. Mater. **163**, 251 (2009)
48. D. Lincot, R.O. Borges, J. Electrochem. Soc. **139**, 1880 (1992)
49. R. Kainthla, D. Pandya, K. Chopra, J. Electrochem. Soc. **127**, 277 (1980)
50. H. Maghraoui-Meherzi, T. Ben Nasr, N. Kamoun, M. Dachraoui, Acad. Sci. Ser. IIc Chim. **14**, 471 (2011)
51. S. Sharma, P. Kumar, R. Thangaraj, Curr. Appl. Phys. **13**, 731 (2013)
52. S. Mahmoud, F. Sharaf, FIZIKA A. **5**, 205 (1996)
53. O. Madelung, *R. Poerschke Data in Science and Technology: Semiconductors Other than Group IV Elements and III–V Compounds*. (Springer-Verlag, Berlin, 1992)
54. A. Mami, I. Mellouki, M.B. Mbarek, M. Amlouk, N. Yacoubi, IEEE Sens. J. **16**, 8374 (2016)
55. C. Wang, A. Mandelis, Rev. Sci. Instrum. **70**, 2372 (1999)
56. K. Biswas, L.D. Zhao, M.G. Kanatzidis, Adv. Energy Mater. **2**, 634 (2012)
57. D.-A. Borca-Tasciuc, G. Chen, A. Prieto, M.S. Martín-González, A. Stacy, T. Sands, M. Ryan, J. Fleurial, Appl. Phys. Lett. **85**, 6001 (2004)